Journal of Applied Physics

RESEARCH ARTICLE | OCTOBER 12 2007

Effect of bifurcation angle in tree-shaped microchannel networks

Xiang-Qi Wang; Arun S. Mujumdar; Christopher Yap

Check for updates

J. Appl. Phys. 102, 073530 (2007)
https://doi.org/10.1063/1.2794379

View Online Export Citation

Articles You May Be Interested In

Vascularization with trees that alternate with upside-down trees

J. Appl. Phys. (May 2007)

Constructal dendritic geometry and the existence of asymmetric bifurcation

J. Appl. Phys. (December 2006)

Flow and heat transfer performance of asymmetric fractal tree network in fractal porous media

Physics of Fluids (February 2024)

13 June 2025 11:14:18

AIP Publishing

Journal of Applied Physics
Special Topics
Open for Submissions
Learn More
AIP Publishing

Effect of bifurcation angle in tree-shaped microchannel networks

Xiang-Qi Wang, Arun S. Mujumdar,[a] and Christopher Yap
Department of Mechanical Engineering, National University of Singapore, 10 Kent Ridge Crescent, Singapore 119260, Singapore

(Received 11 June 2007; accepted 14 August 2007; published online 12 October 2007)

Tree-shaped microchannel networks are being considered for thermal designs that require high heat transfer densities for the cooling of modern electronics. Here we investigate the effect of the bifurcation angles in the constructal nets on the fluid flow and heat transfer characteristics of such networks using a three-dimensional computational fluid dynamics approach. Results show that the bifurcation angle is an important factor which determines the performance of such cooling nets. Surface temperature distributions and pressure drop along the flow paths are analyzed and compared. For the same boundary conditions, a lower temperature and pressure variation is observed at lower bifurcation angles. © *2007 American Institute of Physics*.
[DOI: 10.1063/1.2794379]

I. INTRODUCTION

Compact yet powerful electronic devices are being developed which demand significantly improved cooling designs. Heat sinks embedded with microchannels can be very effective for this application considering their high convective heat transfer coefficients and surface-to-volume ratios. Numerous investigators since Tuckerman and Pease[1] have studied the fluid flow and heat transfer characteristics of microchannels. However, for a series of parallel microchannels, the enhanced heat transfer performance is achieved at the expense of the increased pumping power. Furthermore, the uneven temperature distribution along the heat sinks incorporating straight microchannels is especially undesirable since the significant temperature gradients can result in uneven thermal expansion of the electronic device, possibly damaging it.

The efficient transport characteristics of natural systems provide us with useful hints for the design of an effective microchannel cooling system as noted by Bejan and Errera.[2] They proposed the architecture of "volume-to-point path" so that the flow resistance of the nets is minimal when the network is subjected to two constraints: fixed total volume and fixed channel volume. They found that a tree network has the minimal resistance path. Later, Bejan[3] showed that the total heat flux convected by a double tree is proportional to the total volume raised to power 3/4.

To improve temperature uniformity while decreasing the associated pressure drop, Bejan[4] proposed tree-shaped microchannel networks. Bejan and Errera[5] discussed geometric optimization for channels with fluid flow, specifically for improving temperature uniformity. Later, Pence[6,7] also developed a one-dimensional model to predict the pressure drop as well as the wall temperature distribution along the tree-shaped channel nets using macroscopic correlations. Lower maximum wall temperature and reduced pressure drop were obtained as compared to equivalent straight channel nets using the same length and the same convection surface area. Chen and Cheng[8] also investigated pressure drop and heat transfer characteristics of tree-shaped microchannel nets using several assumptions such as the neglected influence of branching angles and fully developed flow. Similar results were achieved as those of Pence.[6,7]

Disk-shaped heat sinks incorporating tree-shaped microchannel nets were first proposed by Pence.[6] Wechsatol *et al.*[9] investigated optimization of the relevant geometric parameters in such disk-shaped geometry using an analytical approach. The optimized tree-shaped nets can be called "constructal nets" following Bejan's constructal theory.[10] da Silva *et al.*[11–13] also documented superiority of such constructal trees in terms of their thermal performance. Gosselin[14] studied the fundamentals of fluid tree-shaped network optimization under size constraints, viz. surface, volume, and length constraints. The author found an optimal allocation of cost between pumping and size limitation and extended the approach to the design of porous architecture.

Alharbi *et al.*[15,16] carried out a three-dimensional computational simulation for the tree-shaped nets with acute branching angles. They found that the pressure drop of the tree-shaped nets is relatively lower than that of corresponding parallel straight channel nets. The recent study of Wang *et al.*[17] showed that the 90° bifurcation angle case results in a higher pressure drop than that with acute angle bifurcations. Clearly, the bifurcation angle is an important factor during the optimized design of tree-shaped microchannel cooling networks. Bello-Ochende *et al.*[18] presented a numerical and theoretical investigation on geometric optimization of a three-dimensional microchannel heat sink. They found that the degrees of freedom have a strong effect on the peak temperature and the maximum thermal conductance. Tree-shaped channels with heat convection have also been simulated numerically by Dai *et al.*,[19] Tang *et al.*,[20] and Wang *et al.*[21] Recently, a comprehensive review on the constructal theory was conducted by Bejan.[22]

This study was undertaken to obtain an understanding of the effect of the bifurcation angles on the fluid flow and heat transfer characteristics of the tree-shaped nets using three-

[a]Author to whom correspondence should be addressed. Telephone: +65-6874-4623. FAX: +65-6779-1459. Electronic mail: mpeasm@nus.edu.sg

13 June 2025 11:14:18

 © 2007 American Institute of Physics

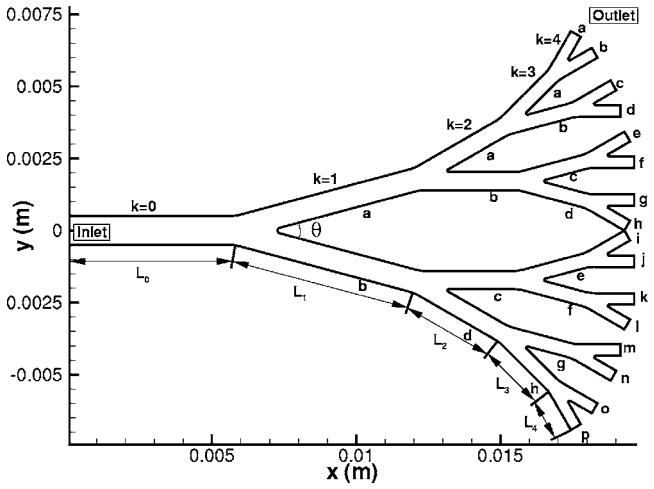

(a) Whole region

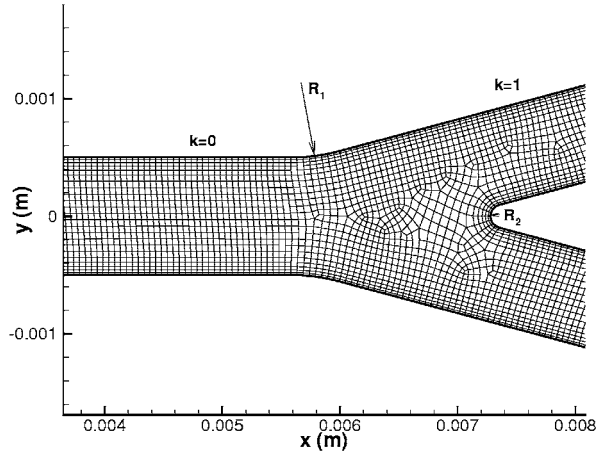

(b) Zoomed region around the bifurcation

FIG. 1. Typical physical model of tree-shaped microchannel channel network ($\theta=30°$).

dimensional computational fluid dynamics approach. This subject was also treated numerically by Wechsatol *et al.*[23] Compared with the previous work of Chen and Cheng,[8] fewer assumptions are made to provide better predictions using computational fluid dynamics. The present computational study removes the assumptions such as the neglect of the effect of bifurcation on heat transfer and pressure drop, and fully thermally and hydrodynamically developed flow. Here the steady Navier–Stokes and energy equations are numerically solved in three dimensions in conjunction with a constant heat flux boundary condition applied at the channel walls.

II. MODEL AND ANALYSIS

Based on the suggestion made by West *et al.*[24] for two-dimensional flow networks, Pence[6] and Wechsatol *et al.*[25] developed a preliminary branching channel network in a disk-shaped heat sink using the following branching ratios:

$$\frac{D_{k+1}}{D_k} = n^{-1/3}, \tag{1}$$

$$\frac{L_{k+1}}{L_k} = n^{-1/2}, \tag{2}$$

where D is the hydraulic diameter, L is the length of a channel segment, and n is the number of branches into which each channel splits. In the present analysis, we use $n=2$. Subscript k represents the lower-order branching level at a given bifurcation. It should be noted that the design in Eqs. (1) and (2) is an assumed rule rather than optimized result. Hence, the fluid flow and heat transfer performance of such designs are significantly below that of optimized trees on disk. Note from Fig. 1(a), that the first branch emanating from the inlet flow plenum is the zeroth-order branch, i.e., for this branch $k=0$. The shaded region and the letters denoted in the figure are discussed later. It was noted by Pence and Enfield[26] that there is a major problem in going to high branching levels using hydraulic diameters in the branching ratio definition to characterize rectangular channels of fixed channel height. Hence, following their suggestion, in the current study a fixed width ratio was employed to circumvent this problem. Thus,

$$\frac{w_{k+1}}{w_k} = n^{-1/3}. \tag{3}$$

Dimensions of the flow network are summarized in Table I. Note that the total channel length reported for the tree-shaped flow network is the sum of the channel segment length ($L_{\text{tot}}=\Sigma_{k=0}^{4}L_k=20$ mm). Various bifurcation angles were used in the parametric study to investigate their effect on the fluid flow and heat transfer characteristics of the channel nets.

As shown in Fig. 1, the channel wall is subjected to a constant heat flux of strength q_0''. The channel is cooled by a single-phase fluid at T_0, which is forced into the channel by a specified mass flow ($\dot{m}$). The coolant is modeled as a New-

TABLE I. Channel dimensions for tree-shaped flow network ($L_{\text{tot}}=20$ mm).

k	h_k (mm)	w_k (mm)	D_k (mm)	L_k (mm)
0	0.50	1.000	0.667	7.12
1	0.50	0.794	0.613	5.02
2	0.50	0.630	0.557	3.56
3	0.50	0.500	0.500	2.52
4	0.50	0.397	0.442	1.78

TABLE II. Properties of liquid water at 1 atm ($273.15 \le T \le 373.15$).

Density, ρ_f (kg/m^3)	$914.56+1.30T-0.036T^2$
Dynamic viscosity, μ_f (Pa s)	$0.458-5.29\times10^{-3}T+2.30\times10^{-5}T^2$ $-4.45\times10^{-8}T^3+3.24\times10^{-11}T^4$
Thermal conductivity, k_f (W/m K)	$-0.794+7.628\times10^{-3}T-9.866\times10^{-6}T^2$
Specific heat capacity, $c_{p,f}$ (J/kg K)	$1089.03-58.15T+0.166T^2-1.55\times10^{-4}T^3$

13 June 2025 11:14:18

TABLE III. Properties of solid (silicon) ($T=310$ K).

Density, ρ_s (kg/m^3)	2330
Thermal conductivity, k_s (W/m K)	125
Specific heat capacity, $c_{p,s}$ (J/kg K)	700

tonian fluid with the temperature-dependent properties given in Table II. The properties of the solid wall (silicon) are assumed constant at $T=310$ K, as shown in Table III. The numerical simulations were conducted using FLUENT 6.2 (Ref. 27), which is a CFD code based on the finite volume method. A steady, incompressible, and laminar flow is considered. The equations in vector notation for the steady-state conservation of mass, momentum, and energy are as follows:

$$\frac{\partial V_i}{\partial x_i} = 0, \tag{4}$$

$$\rho\left[\frac{\partial (V_i V_j)}{\partial x_i}\right] = \frac{\partial}{\partial x_i}\left(\mu \frac{\partial V_j}{\partial x_i}\right) - \frac{\partial p}{\partial x_i}, \tag{5}$$

$$\rho\left[\frac{\partial (V_i c_p T)}{\partial x_i}\right] = \frac{\partial}{\partial x_i}\left(\lambda \frac{\partial T}{\partial x_i}\right). \tag{6}$$

The computational domain marked with the coordinate system $(x-, y-, z-)$ in Fig. 1 has three sections: the heat sink (in silicon) at the bottom (gray shaded part), the constructal channel networks embedded in the sink (black shaded part), and the chip at the top attached to the heat sink (transparent part). In the present analysis, the radius of the fixed heat sink and chip is 20 mm and the total surface area of channel nets (S) is 4×10^{-4} m^2.

As shown in Fig. 1, the flow emanates from the center of the disk to the point at the perimeter of the disk. The related boundary conditions are as follows:

- Inlet: Mass flow inlet ($\dot{m}$), $\dot{m}=1$ g/s is the mass flow rate as inlet boundary condition of the computational domain. Note that the corresponding Reynolds number is around 200 at the inlet and a typical Knudsen number value is about 0.0015.
- Outlet: Pressure outlet. The reference pressure is atmosphere pressure.
- Along the wall of the channel, a constant heat flux of $q''=10$ W/cm^2 is applied; other walls are specified to be adiabatic.

Grid independence of the final results was checked for each geometry. The final grid system used here is about 24 $\times$mod(L_k/0.05 mm)$\times$mod(L_k/0.05 mm). The total number of meshes is around 0.5×10^6 for the studied cases. Convergence was achieved when a maximum residual tolerance of 10^{-6} was reached.

III. RESULTS AND DISCUSSION

Three-dimensional computational results are carried out to predict the fluid flow and heat transfer characteristics through tree-shaped flow networks with various bifurcation angles. To simplify the problems, flow networks rather than heat sinks are discussed.

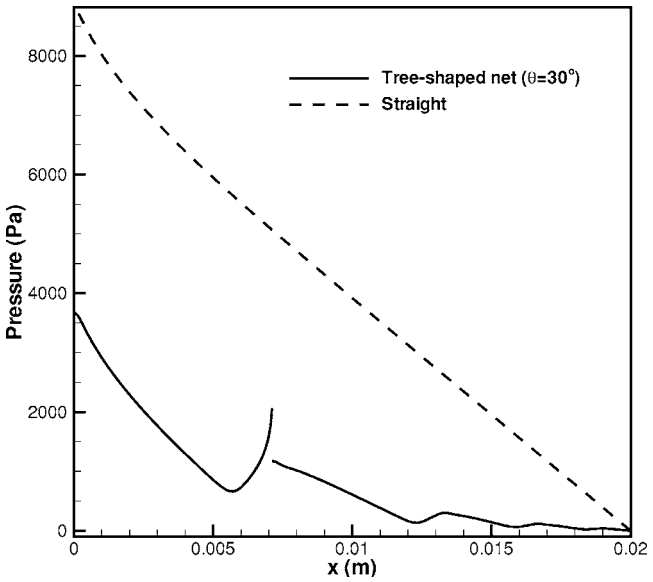

FIG. 2. Centerline pressure distribution along one of the flow path of tree-shaped net ($\theta=30°$) and straight channel.

Comparison of the pressure drop between straight channels and tree-shaped nets was previously analyzed by Pence[7] and Wang.[28] They found that the pressure drop through the tree-shaped nets is relatively lower than that through the straight channels, given the identical total convective surface area and mass flow inlet. To verify the validity of our methods, the results of the tree-shaped nets are compared with those for straight nets. The difference is that rather than the identical total convective surface area, the inlet cross-sectional area was fixed to be the same for the two channel nets. This means that, with the same mass flow inlet, the Reynolds number is also the same. Figure 2 shows the results of comparison of the centerline pressure distribution between

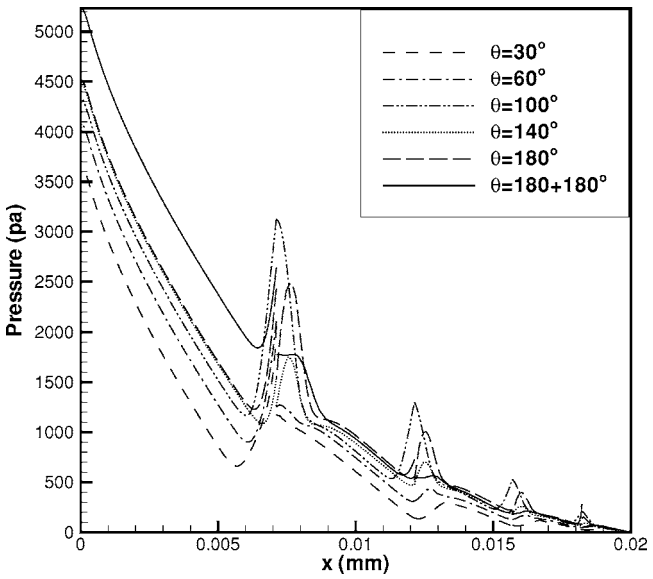

FIG. 3. Pressure distribution along one path ($k=0$, $k=1a$, $k=2a$, $k=3a$, and $k=4a$) of the tree-shaped nets.

13 June 2025 11:14:18

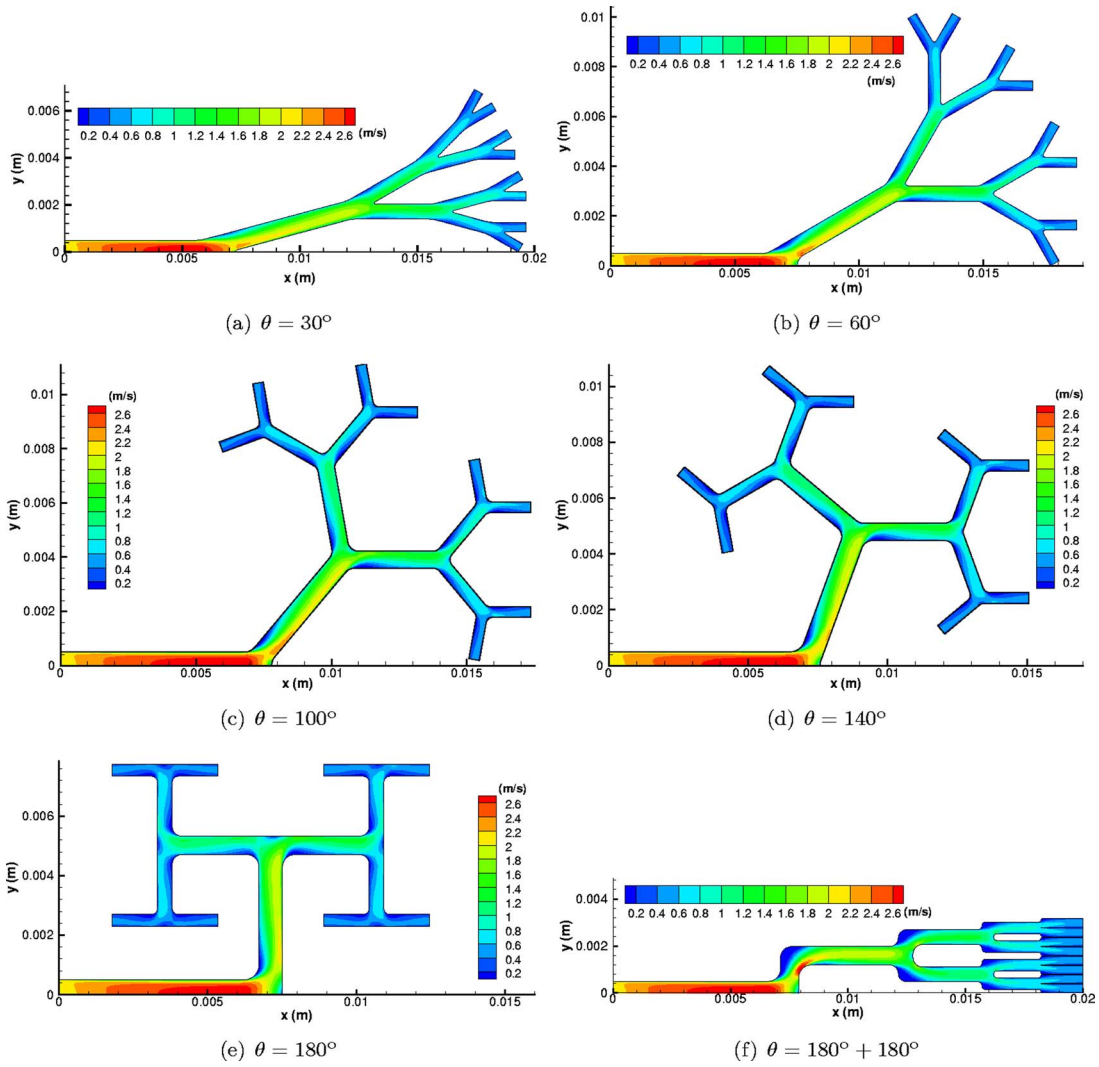

FIG. 4. (Color online) Velocity contours for various angles θ.

the straight channel and one case of the tree-shaped net with θ=30°. For the tree-shaped net, the flow path is defined in Fig. 1(a) by the following branches: k=0, k=1a, k=2a, k=3a, and k=4a. Note that each branching level is presented by a number, i.e., k=0 is the original branch, and each branch segment of each level beyond k=0 is noted by the branch level as well as a letter, a, b, c, etc. in clockwise direction. From the three-dimensional simulations, the pressure drop through the straight channel is about 5130 Pa higher than that through the tree-shaped net, whose value is

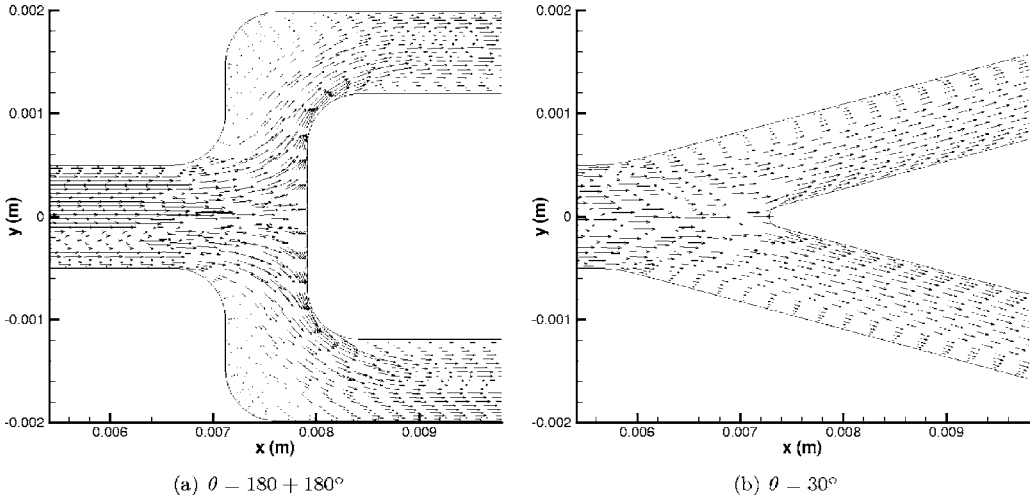

FIG. 5. Vector distribution for two typical cases: θ=30° and θ=180°+180°.

13 June 2025 11:14:18

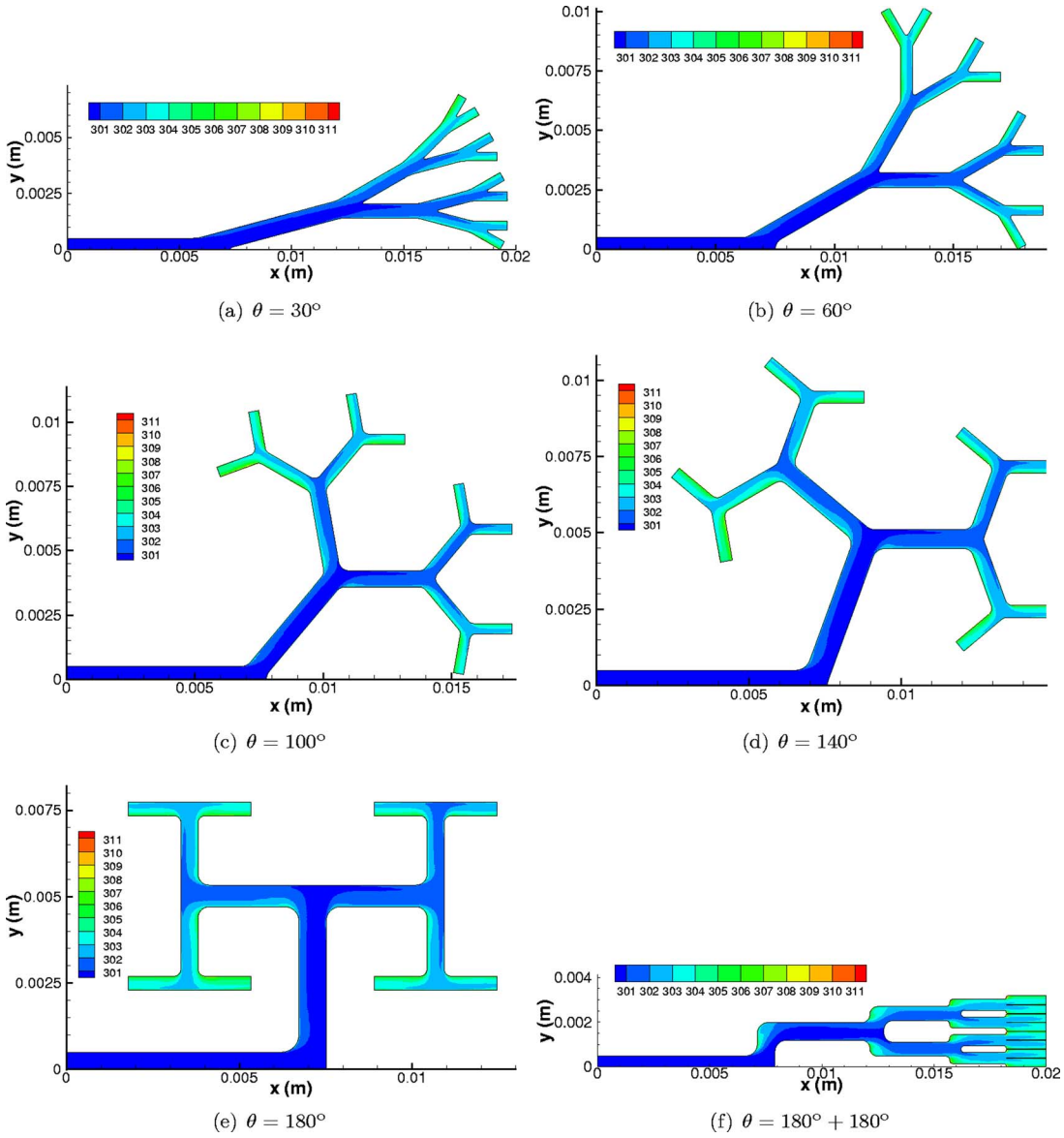

FIG. 6. (Color online) Isotherm contours at bottom surface for various angles of bifurcation. (Unit of temperature is Kelvin.)

around 3670 Pa. As observed from this figure, for the tree-shaped net, there are local pressure spikes at the each bifurcation as expected. With such local changes of pressure, the total pressure drop can decrease significantly. This is an important advantage of such constructal nets.[10]

The bifurcation angle is one of the important geometric parameters of the tree-shaped nets. To clarify the effect of the bifurcation angle, it is necessary to investigate the tree-shaped nets of several angles. Here, to simplify the problem, the bifurcation angles for each bifurcation were fixed to have the same value of θ. In the following study, θ ranges from 30° to 180°, as shown in Fig. 3. Also, a case with a bifurcation angle of (180°+180°) is included. It is found that the pressure drop increases with increasing bifurcation angle. For a low bifurcation angle θ=30°, the total pressure drop is about 3.6 kPa, which is lower than that for the cases with higher bifurcation angles as well as the straight channel. It is also observed that for all the tree-shaped nets, the local pressure spikes at each bifurcation, especially for the low branch levels. Such a sharp increase and decrease of local pressure acts as a buffer to diminish the overall pressure drop. Hence, even for the case of bifurcation angle of (180°+180°), the total pressure (around 5.2 kPa) is lower than that for the straight channel (about 8.8 kPa).

As seen from Fig. 3, except the last case, the pressure drop difference between two adjacent cases is reduced with the increase of the bifurcation angle. For example, when θ changes from 30° to 60°, the increase of the pressure drop is about 0.4 kPa. However, when θ changes from 140° to 180°, the increase of the pressure drop is relatively small and only around 26 Pa. It is clearly seen that smaller θ results in a better performance in terms of the pressure drop. This is a contradiction since in practice a bifurcation angle has to be used to obtain uniform distribution of channel nets in heat sinks. The deterioration of the pressure drop for high bifurcation angles is considered acceptable as compared to the straight case. To explain the observed pressure recovery, details of the flow characteristics are investigated further.

13 June 2025 11:14:18

Details of the flow field of the various tree-shaped nets are investigated to gain better insight into the flow phenomena responsible for the observed spike of pressure. The velocity distributions along the flow path for various bifurcation angles are shown in Figs. 4(a)–4(f). Considering the symmetry of the geometry, only the top half parts are displayed in these figures. Note that in present study, small fillets (not optimized) at each bifurcation (refer to Fig. 1) are used to streamline the fluid flow. As seen from the figures, for all θ, the common feature is that, except for the branch level $k=0$, the fluid flow travels closer to the inner wall; this is due to the inertia of the flowing fluid. For $\theta=30°$ [Fig. 4(b)], at the first bifurcation position between $k=0$ and $k=1$, a stagnation point is caused by the bifurcating point. Hence, development of a new laminar boundary layer is clearly noted at the inner wall at $k=1$ branch. Similar phenomena occur at other branch levels. Due to the rebuilding of the laminar boundary layer at each branch level, the local pressure can be recovered at each bifurcation point which results in a decrease of the global pressure drop.

Although fillets were used at the bifurcations, the nonuniformity is noticeable near the junctions, especially at high bifurcation angles. For example, as seen in Fig. 4(f), for $\theta=180°$, the change of channel direction results in a sharp change of the flow direction from horizontal to vertical. Hence, the stagnation of the fluid at the inner wall of the bifurcations causes a low velocity and high pressure spot to develop. Furthermore, due to the large change of bifurcation angles, the flow acts as an interference on the plane and results in local recirculation of the flow at the outer corner of the bifurcation with low velocity, which can also be observed in Fig. 5(a) for the $(180°+180°)$ case. With lower bifurcation angle, such a vortex at outer corner is weaker, for example at $\theta=30°$, Fig. 5(b). It should be clarified that in Fig. 4(a), the channel direction changes twice. Hence, the stagnation point occurs at the inner wall of the first bifurcation, which is similar to other cases. However, the second bifurcation plays a role of a step to increase the velocity at the corner appreciably. Due to the sharp change and recovery of the flow direction, the velocity at the outer corner at the bifurcation is much lower than that in other cases. Due to the large change of flow pattern in this net, the resulting pressure drop should be greater, as shown in Fig. 3. Although only the bifurcation between $k=0$ and $k=1$ is discussed here, similar phenomenon occurs at other bifurcations. The only difference is that the magnitude is reduced due to the decreased mean velocity.

As seen from Figs. 4 and 5, the velocity distribution is nonuniform in tree-shaped nets. However, considering the reduced global pressure drop, such flow networks are noticeably better than the conventional straight channel nets. Later, the advantages in heat transfer characteristics also can be found. Note that fabrication of such complex channels will be a challenging microfabrication task.

Figures 6(a)–6(f) display the predicted temperature distributions over the bottom surface of the networks for various angles. Globally the maximum temperature is of similar magnitude for all the cases studied and occurs at the outer wall near the outlets. This is easily explained since the fluid has the lowest velocity here (refer to Fig. 6). The high temperature spot should be noted since it is related to the quality of the cooling network. For $\theta=30°$, the high temperature spot only occurs at the high-level branches, which is caused by the reduced velocity and redevelopment of laminar boundary layers. When the bifurcation angle is increased to $\theta=60°$, the local high temperature spot can be observed at the initial stage of $k=1$, although the magnitude is not very large. With further increase of the bifurcation angle, the high temperature spot is more noticeable near the outer corner of each bifurcation. Especially for the case $\theta=180°+180°$, it is the most serious. Due to the recirculation of fluid flow in the outer corner near each bifurcation, the temperature is relatively higher as compared to the bulk fluid temperature. Such a high temperature spot is not desirable in practice. Fortunately, such a hot spot can be alleviated using an optimized streamlined design of bifurcation structure, which needs further investigation.

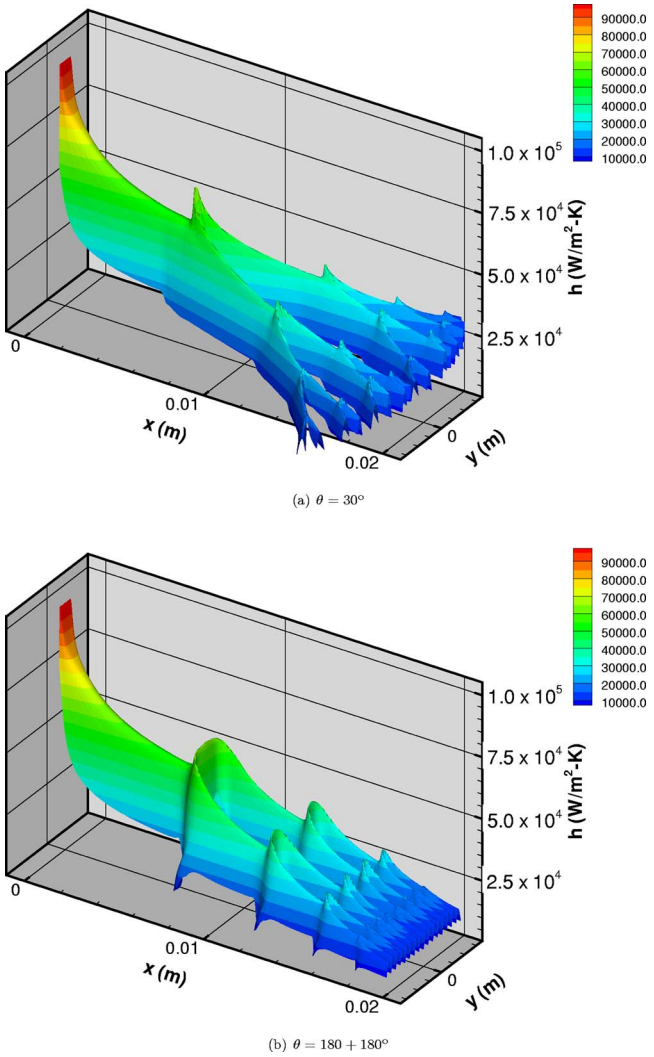

FIG. 7. (Color online) Heat transfer coefficient contours for various angles.

The heat transfer characteristics also can be examined in terms of the distribution of heat transfer coefficients. Figure 7 shows the local heat transfer coefficient (h') contours at the bottom surface for two typical bifurcation angles: $\theta=30°$ and $\theta=180°+180°$. With respect to the temperature distribution

13 June 2025 11:14:18

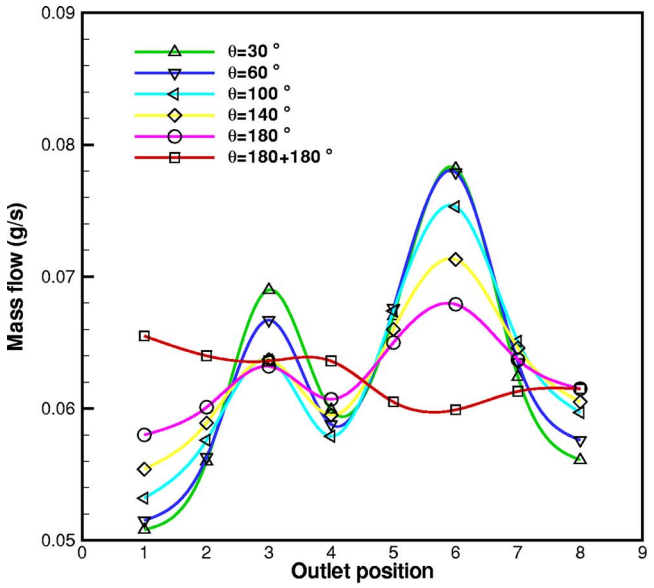

(a) Mass flow

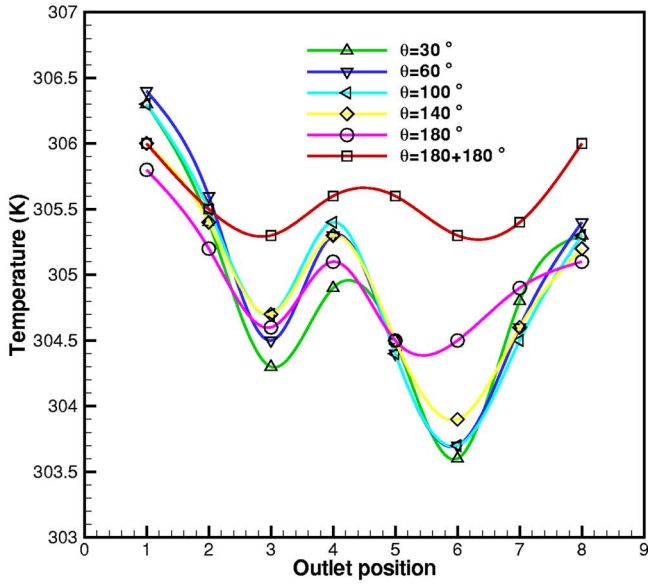

(b) Temperature

FIG. 8. (Color online) Mass flow (a) and bulk temperature (b) distribution at the outlet positions.

discussed previously, the h' contours show similar trends. The local heat transfer coefficient spikes at each bifurcation with different magnitude. Such local recovery of heat transfer coefficients can contribute to the global increase of heat transfer coefficients.

Finally, to highlight the influence of bifurcation angles on the thermal and flow conditions through tree-shaped network, outlet mass flow values ($\dot{m}_{\text{out}}$) and the outlet bulk fluid temperatures T_{out} are shown in Figs. 8(a) and 8(b), respectively. Considering the symmetry of the structure, only the top half outlets are shown here, which are denoted from 1 to 8, corresponding to $a-h$ of Fig. 1(a). The symbols are connected using a spline curve to show the trend clearly. For the exit mass flow, it is found that for various angles from 30° to 180°, the maximum value occurs at outlet $k=4f$. It is reasonable when checking the geometry structure in Fig. 1(a). Path $k=0$, $k=1a$, $k=2b$, $k=3c$, and $k=4f$ has the minimum global angle (referred to the horizontal x axis). The second large value occurs at the outlet $k=4c$, corresponding to the path $k=0$, $k=1a$, $k=2a$, $k=3b$, and $k=4c$. It is clear that the outlet at the inner part of the flow has the higher mass flow. Hence, the trend line in the figure shows clearly sinusoidal behavior. It is noted that more uniform distribution of the outlet mass flow can be achieved with increased bifurcation angles, but the gradient is reduced with increasing angles. However, the case of $\theta=180°+180°$ needs to be considered separately. As shown in Fig. 8(a), this case has the most uniform distribution of outlet mass flow. The reason is that for this net, the centerline angle between different subchannels is zero. Also, the displacement of the outlet position from $y=0$ explains the reason for nonuniformity of the mass flow distribution.

Similarly, corresponding to the fluid flow feature, the bulk fluid temperature distribution in Fig. 8(b) can be easily understood. The lowest exiting bulk temperature at the outlet $k=4f$ is expected due to the highest flow rate there.

IV. CONCLUSION

In this study, fluid flow and heat transfer through tree-shaped branching flow networks were examined using a three-dimensional CFD analysis. Results of pressure distribution through tree-shaped nets with various bifurcation angles as well as straight channels are compared and analyzed. Results indicate that the global pressure drop increases with the increase of bifurcation angle, although it is much smaller as compared to that of straight net. Furthermore, the increased bifurcation angle deteriorates the flow field as well as the thermal patterns. Hence, the tree-shaped net with small bifurcation angle is desired in practice, although the uniform distribution of nets over a provided heat sink has to be considered.

[1]D. B. Tuckerman and R. F. W. Pease, IEEE Electron Device Lett. **EDI-2**, 126 (1981).
[2]A. Bejan and M. R. Errera, Fractals **5**, 685 (1997).
[3]A. Bejan, Int. J. Heat Mass Transfer **44**, 699 (2001).
[4]A. Bejan, Int. J. Heat Mass Transfer **40**, 799 (1997).
[5]A. Bejan and M. R. Errera, Int. J. Heat Mass Transfer **43**, 3105 (2000).
[6]D. V. Pence, *Proc. International Conference on Heat Transfer and Transport Phenomena in Microscale* (Banff, Canada, 2000), pp. 142–148.
[7]D. V. Pence, Microscale Thermophys. Eng. **6**, 319 (2002).
[8]Y. Chen and P. Cheng, Int. J. Heat Mass Transfer **45**, 2743 (2002).
[9]W. Wechsatol, S. Lorente, and A. Bejan, Int. J. Heat Mass Transfer **45**, 4911 (2002).
[10]A. Bejan, *Shape and Structure, From Engineering to Nature* (Cambridge University Press, Cambridge, 2000).
[11]A. K. da Silva, S. Lorente, and A. Bejan, J. Appl. Phys. **96**, 1709 (2004).
[12]A. da Silva and A. Bejan, Int. J. Heat Fluid Flow **26**, 34 (2005).
[13]A. da Silva, S. Lorente, and A. Bejan, Int. J. Heat Mass Transfer **48**, 2662 (2005).
[14]L. Gosselin, Int. J. Therm. Sci. **46**, 434 (2007).
[15]A. Y. Alharbi, D. V. Pence, and R. N. Cullion, J. Fluids Eng. **125**, 1051 (2003).
[16]A. Y. Alharbi, D. V. Pence, and R. N. Cullion, J. Heat Transfer **126**, 744 (2004).
[17]X.-Q. Wang, C. Yap, and A. S. Mujumdar, J. Electron. Packag. **128**, 273 (2006).
[18]T. Bello-Ochende, L. Liebenberg, and J. Meyer, Int. J. Heat Mass Transfer **50**, 4141 (2007).
[19]W. Dai, A. Bejan, X. Tang, L. Zhang, and R. Nassar, J. Appl. Phys. **99**,

13 June 2025 11:14:18

104702 (2006).
[20]X. Tang, W. Dai, R. Nassar, and A. Bejan, Numer. Heat Transfer, Part A **50**, 809 (2006).
[21]H. Wang, W. Dai, and A. Bejan, Int. J. Heat Mass Transfer **50**, 1843 (2007).
[22]A. Bejan and S. Lorente, J. Appl. Phys. **100**, 041301 (2006).
[23]W. Wechsatol, S. Lorente, and A. Bejan, Int. J. Heat Mass Transfer **49**, 2957 (2006).
[24]G. B. West, J. H. Brown, and B. J. Enquist, Science **276**, 122 (1997).
[25]W. Wechsatol, A. Bejan, and S. Lorente, Numer. Heat Transfer, Part A **48**, 731 (2005).
[26]D. V. Pence and K. E. Enfield, in *Design and Nature*, edited by C. M. C. Brebbia (WIT, Rhodes, Greece, 2004), pp. 317–328.
[27]www.fluent.com, FLUENT Inc., Lebanon, NH, USA, 2006.
[28]X.-Q. Wang, A. S. Mujumdar, and C. Yap, J. Electron. Packag. **128**, 38 (2006).

13 June 2025 11:14:18